

Relativistic Particle Acceleration in a Folded Current Sheet

S. Zenitani and M. Hoshino

Department of Earth and Planetary Science, University of Tokyo, 7-3-1, Hongo, Bunkyo, Tokyo, 113-0033 Japan; zenitani@eps.s.u-tokyo.ac.jp

ABSTRACT

Two-dimensional particle simulations of a relativistic Harris current sheet of pair (e^\pm) plasmas have demonstrated that the system is unstable to the relativistic drift kink instability (RDKI) and that a new kind of acceleration process takes place in the deformed current sheet. This process contributes to the generation of non-thermal particles and contributes to the fast magnetic dissipation in the current sheet structure. The acceleration mechanism and a brief comparison with relativistic magnetic reconnection are presented.

Subject headings: acceleration of particles — instabilities; plasmas — relativity; magnetic fields — pulsars(individual: Club Pulsar)

1. Introduction

A current sheet structure with reversed magnetic fields can be seen everywhere in the universe. Among the magnetic field dissipation processes in the current sheet, magnetic reconnection may be the most popular one. Breaking the topology of magnetic field lines, it releases the magnetic energy into particles' kinetic energy in a relatively short time scale (several to several tens of an Alfvén transit time $\tau_A = \lambda/V_A$, where λ is the half thickness of the current sheet and V_A is the typical Alfvén speed). It plays an essential role in solar terrestrial sites such as the Earth's magnetotail (Dungey 1961) and source regions of the solar flare (Parker 1957). Moreover, it is expected in astrophysical sites such as AGNs (Lesch & Birk 1998; Schopper et al. 1998) and pulsar winds, especially their well-studied example of the Crab Nebula (Coroniti 1990). In case of the Crab Nebula, energy conversion in a relativistic wind of e^\pm plasmas has been a long-standing problem (Kennel & Coroniti 1984; Coroniti 1990; Lyubarsky & Kirk 2001; Kirk & Skjæraasen 2003) (so-called the “ σ -problem”, where σ is the ratio of the Poynting flux energy to the particle kinetic flux). The wind is originally poynting-dominated ($\sigma \sim 10^4$) close to the neutron star (Arons 1979), while it is kinetic-dominated near the termination shock (σ is far less than the unity; $\sigma \sim 10^{-3}$ by

Kennel & Coroniti (1984), $\sigma \sim 10^{-1}$ by Mori et al. (2004)). Recently, relativistic magnetic reconnection in the striped current sheets has been discussed as the most possible dissipation mechanism (Coroniti 1990; Lyubarsky & Kirk 2001; Kirk & Skjæraasen 2003). The properties of relativistic reconnection in e^\pm plasmas have been investigated by an analytical study (Blackman & Field 1994) and by computer simulations (Zenitani & Hoshino 2001; Jaroschek et al. 2004). One of the most important features of relativistic reconnection is the generation of non-thermal particles due to a direct acceleration by dc electric field around the X-type region (Zenitani & Hoshino 2001). However, the above discussion is based on a 2D picture of reconnection. Instabilities in a cross-field plane are also of critical importance to understand a realistic current sheet problem including reconnection. Does reconnection grow faster than cross-field instabilities? Is reconnection the fastest dissipation process? In case of non-relativistic ion-electron plasmas, the following instabilities have been discussed: the lower hybrid drift instability (LHDI) (Krall 1971; Davidson et al. 1977), the Kelvin-Helmholtz instability (KHI) (Yoon & Drake 1996; Shinohara et al. 2001), and the drift kink instability (DKI) (Zhu & Wing 1996; Pritchett et al. 1996; Daughton 1998). They lead to plasma heating and particle acceleration as well as triggering of reconnection. A purpose of this paper is to search basic properties of such cross-field instabilities and non-thermal particle generation in a relativistic e^\pm current sheet. In this letter, we report our 2D simulations in a cross-field plane of a relativistic e^\pm current sheet and we report a new acceleration process related to the relativistic drift kink instability (Zenitani & Hoshino 2003).

2. Simulation

The simulation code used here is a 3D particle-in-cell code. The system size is 1 (X) $\times 256$ (Y) $\times 512$ (Z) grids. We consider periodic boundaries in the X, Y directions, while we periodically set two simulation boxes in the Z direction. The typical scale of the current sheet λ is set to 10 grids, so that the Y boundaries are located at $y = \pm 12.8\lambda$, and the Z boundaries in each simulation boxes are at $z = \pm 12.8\lambda$. We take the relativistic Harris model as the initial current sheet. The magnetic field, the density of plasmas and their distribution functions are described by $\mathbf{B} = B_0 \tanh(z/\lambda) \hat{\mathbf{x}}$, $n(z) = n_0 \cosh^{-2}(z/\lambda)$ and $f_\pm \propto n(z) \exp[-\Gamma_\beta \{\varepsilon - \beta_\pm u_y\}/T]$. In the above equations, B_0 is the magnitude of magnetic field in the lobe (background region), n_0 is the number density of plasmas in the current sheet, $\beta_\pm = v_\pm/c$ are the drift velocities for each species; $\beta_+ = +\beta$ for positrons, $\beta_- = -\beta$ for electrons, Γ_β is the Lorentz factor for β ($\Gamma_\beta = [1 - \beta^2]^{-1/2}$), ε is the particle energy, \mathbf{u} is the relativistic four velocity of $\mathbf{u} = [1 - (v/c)^2]^{-1/2} \cdot \mathbf{v}$ and T is the temperature. In the first simulation, we set $T = mc^2$ and $\beta = 0.3$. We set no driving force to excite instabilities, so that instabilities arise from thermal noise. We set no background plasmas. The total energy

is conserved within an error of 0.3% throughout the simulation run.

3. Results

Snapshots at three characteristic stages of the simulation are presented in Fig. 1. Left three panels in Fig. 1 show color contours of the plasma density at (a) $t/\tau_c = 46.0$, (b) 64.0 and (c) 82.0, where time is normalized by the light transit time $\tau_c = \lambda/c$. Panels in the middle column are color contours of the electric field E_y at the corresponding time and white lines show contours of B_x . Panels in the right column are particles’ energy spectra for the whole simulation particles. The horizontal axis shows particles’ energy normalized by mc^2 .

As shown in the top three panels in Fig. 1, we observe a kink-type modulation of the current sheet. We confirmed that this is a signature of the relativistic drift kink instability (RDKI), a relativistic extension of the drift kink instability (DKI), which is a long-wavelength, current-driven instability in a thin current sheet. In the top-center panel, one can see a typical structure of E_y components of polarization electric fields of RDKI. The sign of E_y is positive in yellow regions, while it is negative in blue regions. Two types of regions appear alternatively along the current sheet and they are anti-symmetric with the neutral plane ($z = 0$). Note that the $\mathbf{E} \times \mathbf{B}$ direction using the lobe magnetic fields and the observed sign of E_y is consistent with the Z-displacement of the plasma bulk motion. The symmetric E_z components are also observed and their values are little less than or comparable with those of E_y . The E_x components are negligible. Since the system is uniform in the X direction, there is no electrostatic E_x fields. After $t/\tau_c \sim 50$, the instability turns into its non-linear stage. The middle three panels in Fig. 1 are snapshots of the current sheet at $t/\tau_c = 64.0$. The current sheet is strongly folded within the zone of $-4 < z/\lambda < 4$. Due to the Z-displacement by RDKI, red (originally yellow) regions, where $E_y > 0$, are placed in a row around the neutral plane ($z = 0$) in the middle-center panel of Fig. 1. The total kinetic energy in the system has increased by 30% at this time. Importantly, we observe a clear sign of the particle acceleration in a high-energy tail in the energy spectrum of the middle-right panel in Fig. 1. We discuss the acceleration process later. The kinked-shape of the current sheet is not stable, because fragments of the anti-parallel currents ($\pm J_z$) pull each other. As they start to collide, the system turns into the “mixed” stage. The snapshots in this stage are presented in the bottom three panels in Fig. 1 at $t/\tau_c = 82.0$. Due to the enhanced diffusion by sheet collisions, the total kinetic energy has increased by 170% at this time. In the energy spectrum of the right-bottom panel, one can recognize both a remnant of the non-thermal tail and global plasma heating. Finally, the mixed current sheet slowly

evolves into the broaden current sheet, which is 3-4 times thicker than the initial state. The saturated level of total kinetic energy is 330-340% at $t/\tau_c = 200$ or later. The spectrum looks unchanged from the mixed stage; one can still observe the non-thermal tail.

4. Discussion

Now, we again take a look at the instability in its linear stage. The observed growth rate (ω_i/Ω_c) is plotted as a function of $k_y\lambda$ in Fig. 2, where k_y is the wavenumber and Ω_c is the gyro frequency $\Omega_c = \omega_c/\gamma = (eB)/(\gamma mc^2)$. The growth rate and wave-length of the most dominant mode of RDKI is $\omega_i/\Omega_c \sim 0.035$ and $k_y\lambda \sim 1.0$. We have also calculated eigen functions and their growth rates of the RDKI, by linearizing relativistic two-fluid equations. The theoretical growth rates for the present case are shown as a solid line in Fig. 2. The simulation results are consistent with them except for shorter wavelength of $k_y\lambda > 1$, where the instability is suppressed by kinetic effects. We observe a slight signature of the relativistic drift sausage instability (RDSI) along with RDKI. However, RDSI is less influential on the current sheet deformation and particle acceleration. Note that no velocity-shear-driven mode such as KHI is excited, because there is no velocity shear between drifting plasmas in the current sheet and empty background plasmas. Also note that LHDI is not excited in an e^\pm case, because there is no delay of positron's response to electron's.

Next, we discuss an acceleration mechanism, which is found in the non-linear stage of RDKI. By analyzing trajectories of highly-accelerated particles, we found that the main site of particle acceleration is the central channel around $z \sim 0$, where the current sheet was originally located. For simple discussion, we call this channel as the “acceleration channel (AC)”. We illustrate the acceleration mechanism in schematic views in Fig. 3. In the upper view, the structure of polarization E_y fields in the linear stage are illustrated. They are anti-symmetric with respect to Z and both positive and negative regions are alternatively located along the sheet. Passing through their meandering orbits, some particles can resonate with the E_y fields. Some of them gain their energy and others lose their energy. In the non-linear stage, due to the Z -displacement of the current sheet, the positive E_y regions are now located around the AC. Inside the positive E_y regions, typical values of the fields are $|B_x| \approx 0.6 - 0.7B_0$ and $E_y \approx 0.2 - 0.3B_0$. On the contrary to the reconnection (Zenitani & Hoshino 2001; Jaroschek et al. 2004) in which $|E|/|B| > 1$ in an acceleration site, the value of $|E|/|B|$ is less than the unity inside the positive E_y regions and so low-energy particles travel into the $E \times B$ direction. However, fewer population of high-energy particles can travel across the positive E_y regions, because their Larmor radii r_L are larger than the half wavelength of RDKI (π/k_y). They gain their energy from the electric field E_y , cross the

current sheet and move into the neighboring positive E_y regions. Since r_L becomes larger as particles gain more energy ($r_L \propto \varepsilon^{1/2}$ in non-relativistic case and $r_L \propto \varepsilon$ in relativistic case), accelerated particles usually satisfies the crossing condition of $r_L > \pi/k_y$ in the next positive E_y regions. In this way, they are successively accelerated in the AC, passing through multiple positive E_y regions into $\pm Y$ direction. The above condition can be interpreted as “trapping condition” inside the AC. Higher-accelerated particles tend to stay in the AC, because larger r_L prevents them from escaping from the AC. This is why the non-thermal tail is enhanced in the energy spectrum. We think this type of enhanced acceleration can be found in any kink-type instabilities in a thin current sheet, as long as its wavelength is comparable with a particle’s Larmor radius. For example, it may be applicable to acceleration of ions, when a thin current sheet of ion-electron plasmas is modulated by KHI. The folded structure evolves into the mixed stage when its Z-displacement (Δz) is nearly same as the half wavelength of RDKI ($\Delta z \sim \pi/k_y \sim \pi\lambda$). Assuming that v_z is typically $V_{E \times B} \sim 0.3c$ in the positive E_y regions, the time scale of the non-linear stage (τ_N) is approximated by $\tau_N \sim \pi\lambda/v_z \sim 5-10\tau_c$.

After the system turns into the mixed stage, not only few number of high-energy particles but also a lot of low-energy particles in the current sheet interact with the positive E_y regions. Then the magnetic fields are dissipated in a time-scale of tens of τ_c . Roughly speaking, the magnetic field energy is consumed by Joule heating of the E_y fields and the total current \bar{I}_y in the broaden current sheet. The magnetic energy stored between the folded curves is approximated by $(\pi/k_y)B_0^2/8\pi$. We assume that the average value of the electric fields $\bar{E}_y \sim 0.5E_y = 0.5 \times (0.2-0.3)B_0$, where the factor 0.5 represents the fact that positive E_y is not uniform in the AC. The total current \bar{I}_y is represented by the 0th order current $\bar{I}_y \sim \lambda J_0 = cB_0/4\pi$. Thus the dissipation time scale (τ_D) is approximated by $\tau_D \sim (\pi/k_y)(B_0^2/8\pi)(\lambda J_0 \bar{E}_y)^{-1} \sim 10-20\tau_c$.

Next, we briefly compare RDKI and magnetic reconnection (Zenitani & Hoshino 2001). In Table 1, parameters for several simulation runs of RDKI and relevant runs of reconnection are presented. Throughout the simulation runs, we calculate the ratio of the non-thermal kinetic energy to the total kinetic energy (K_{nonth}/K) and their maximum values in time are presented in Table 1. In case of run D3, K_{nonth} is not resolved by our method. The maximum energies (ε_{max}) are also presented in Table 1. In case of RDKI, highest-energy particles run in the AC into the $\pm Y$ direction with the light speed during the non-thermal stage and the mixed stage. Their maximum energies are estimated by $\varepsilon_{est} \sim \varepsilon_{max0} + ec\bar{E}_y(\tau_N + \tau_D) \sim \varepsilon_{max0} + 3\omega_c\tau_c mc^2$ and the estimated values agree with simulation results. In three cases of reconnection, the evolution seems to be restricted by the periodic system size of L_x , because two outflow jets travel into the $\pm X$ direction. Due to this restriction, the upper limits of particle energy are estimated by $\varepsilon_{est} = eB_0L_x/2$ in Table 1 in reconnection cases. However, the obtained maximum energies (ε_{max}) by reconnection are far larger than the

maximum energies by RDKI. On the viewpoint of field dissipation (e.g. striped pulsar winds), RDKI can dissipate more magnetic energy. The linear growth rates of the energy conversion ($\tau_c d \ln(\Delta K) / dt$) are presented in Table 1. Generally speaking, RDKI grows *faster* in a relativistic current sheet ($T/mc^2 \geq 1$) and it converts 2.5 – 3.5 times as many energy as the initial kinetic energy in the current sheet in a time scale of τ_D . Moreover, RDKI spontaneously occurs everywhere in the X direction, while single reconnection requires wide spatial range in the X direction in order that outflow jets can escape. Therefore, even in Runs R3 and D3, in which RDKI grows slower, it takes twice longer time by reconnection to dissipate the same amount of the magnetic energy as RDKI. On the contrary, reconnection is more favorite candidate as an origin of the non-thermal particles. It produces more non-thermal energy of K_{nonth} than RDKI, due to high ratio of K_{nonth}/K .

In 3D situation, our initial results of 3D simulation show that RDKI occurs almost uniformly in the current sheet. Also, Jaroschek et al. (2004) have presented their 3D results of triggered reconnection. They have referred the importance of RDKI in 3D case and a signature of 2D-like RDKI is observed outside the reconnection region. In case of multiple current sheets structure, such as striped pulsar winds, there are several possibilities of enhanced field dissipation. If a distance between two currents is less than the critical distance of $2\lambda_c$, two current sheets collide each other and 90% or more of the magnetic energy can be dissipated into the particle energy. In typical cases, $\lambda_c \sim 7\text{-}8$, but its dependency on T or β should be further investigated. We also note that the secondary RDKI takes place in the broaden current sheet in some occasions.

Let us summarize this paper. First, we investigate the RDKI in a thin e^\pm current sheet. Second, we find a new acceleration process that uses a folded structure of a current sheet. The unique point of this process is that ac electric fields evolve into dc acceleration channel. Third, due to the enhanced acceleration, a non-thermal particles are produced. Fourth, comparison with reconnection shows that RDKI is more favorable to dissipate the magnetic energy in the current sheet structure. We believe that RDKI provides a crucial hint to the energy dissipation problem in the current sheets in the universe, including striped pulsar winds.

This work was supported by facilitates of JAXA and the Solar-Terrestrial Environment Laboratory, Nagoya University.

REFERENCES

J. Arons 1979, Space Sci. Rev., 24, 437

E. G. Blackman and G. B. Field 1994, Phys. Rev. Lett., 72, 494

F. V. Coroniti 1990, ApJ, 349, 538

W. Daughton 1998, J. Geophys. Res., 103, 29429

R. C. Davidson et al. 1977, Phys. Fluids, 20, 301

J. W. Dungey 1961, Phys. Rev. Lett., 6, 47

C. H. Jaroschek, R. A. Treumann, H. Lesch and M. Scholer 2004, Phys. Plasmas, 11, 1151

C. F. Kennel and F. V. Coroniti 1984, ApJ, 283, 694

J. G. Kirk and O. Skjæraasen 2003, ApJ, 591, 366

N. A. Krall 1971, Phys. Rev. A4, 2094

H. Lesch and G. T. Birk 1998, ApJ, 499, 167

Y. Lyubarsky and J. G. Kirk 2001, ApJ, 547, 437

K. Mori, D. N. Burrows, J. J. Hester, G. G. Pavlov, S. Shibata and H. Tsunemi 2004, ApJ, 609, 186

E. N. Parker 1957, J. Geophys. Res., 62, 509

P. L. Pritchett, F. V. Coroniti and V. K. Decyk 1996, J. Geophys. Res., 101, 27413

R. Schopper, H. Lesch and G. T. Birk 1998, A&A, 335, 26

I. Shinohara, H. Suzuki, M. Fujimoto and M. Hoshino 2001, Phys. Rev. Lett., 8709, 5001

P. Yoon and J. F. Drake 1996, J. Geophys. Res., 101, 27327

S. Zenitani and M. Hoshino 2001, ApJ, 562, L63

S. Zenitani and M. Hoshino 2003, Proc. of the 28th ICRC

Z. Zhu and R. M. Winglee 1996, J. Geophys. Res., 101, 4885

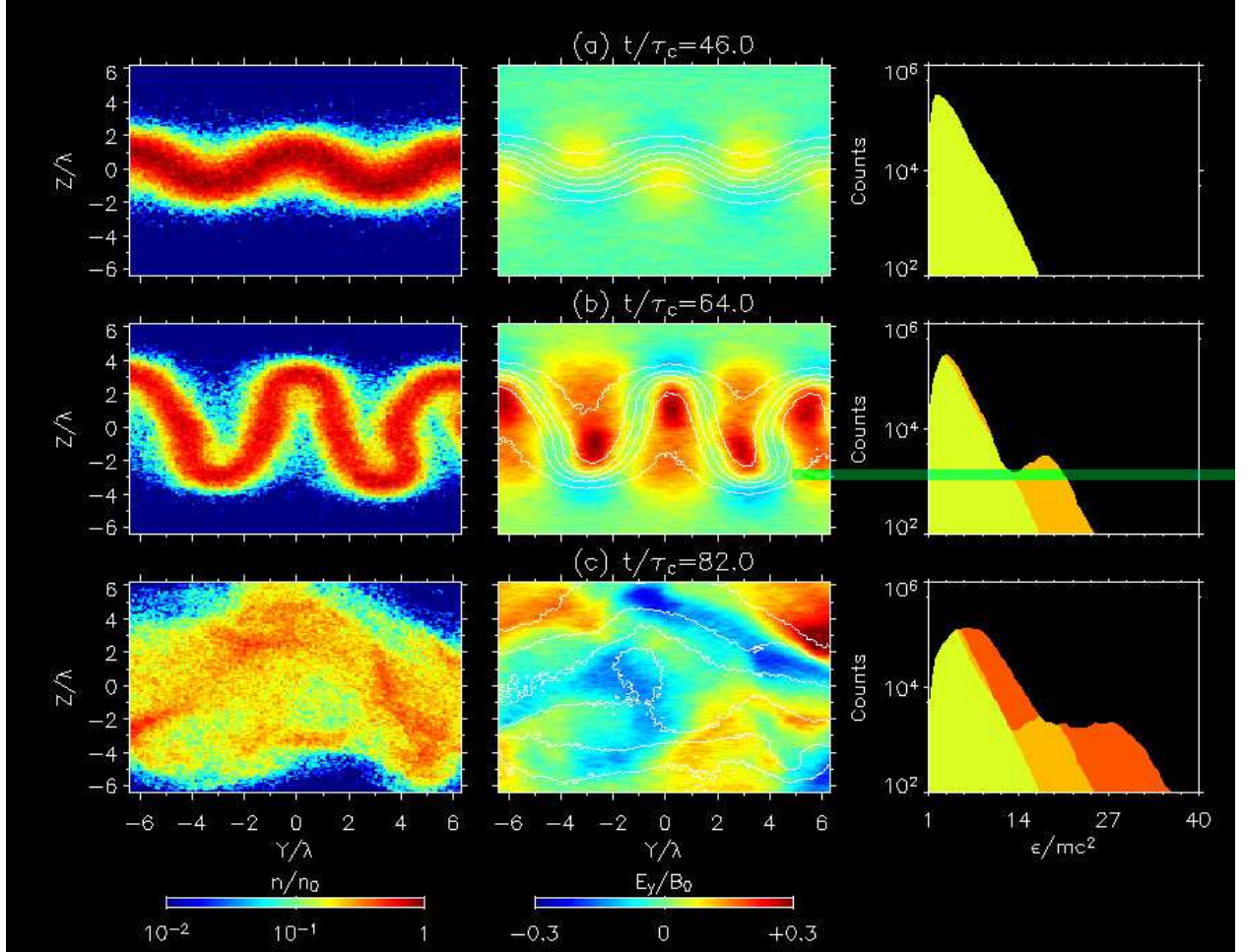


Fig. 1.— (color). Left three panels show color contours of the plasma density at $t/\tau_c = 46.0$, 64.0 and 82.0. Panels in the middle column represent E_y at the corresponding time and white lines shows contours of B_x . Panels in the right column are energy spectra.

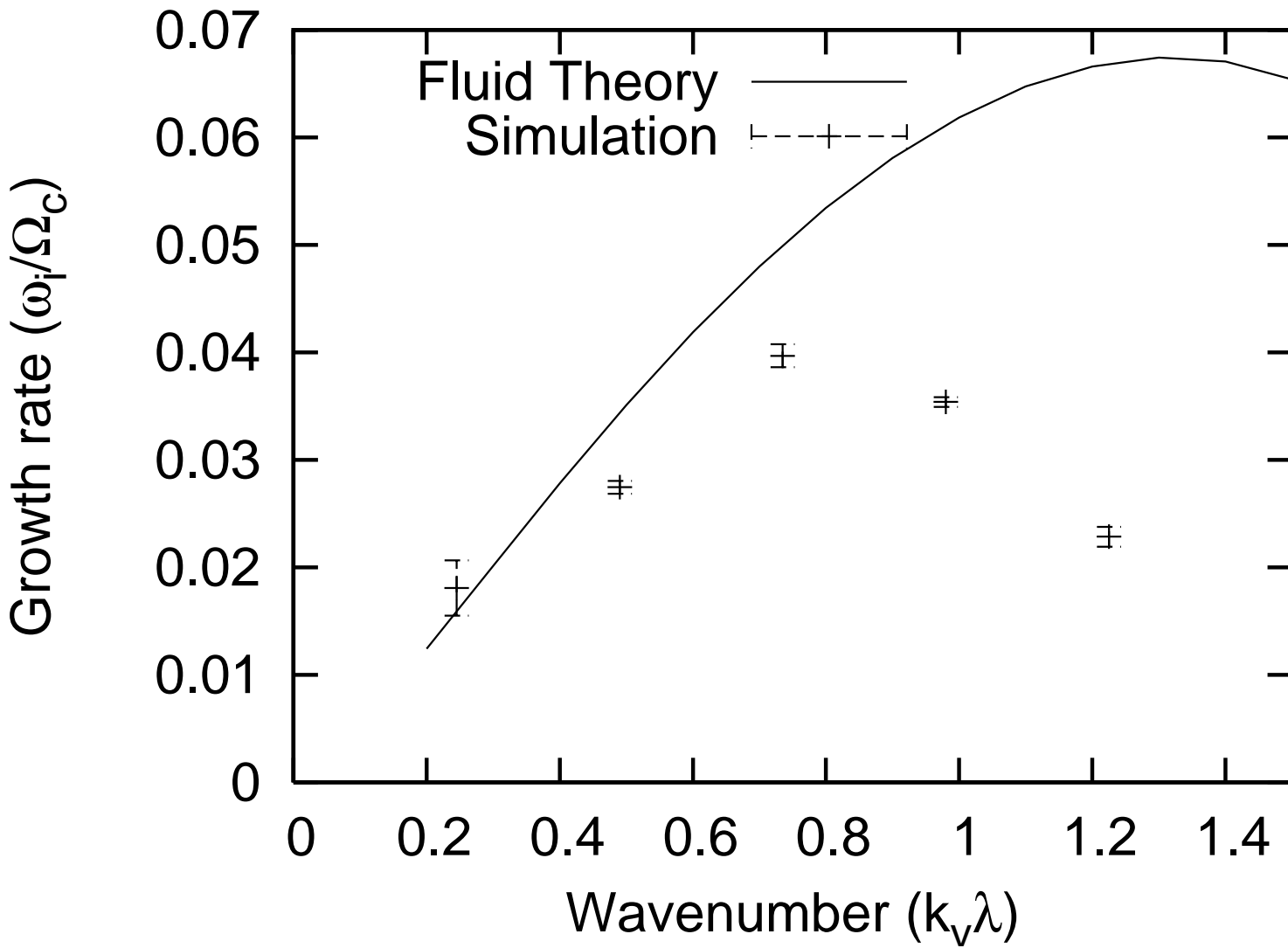


Fig. 2.— Plot of the observed growth rates (ω_i/Ω_c) as a function of the normalized wavenumber ($k_y\lambda$). A solid line shows eigen growth rate predicted by relativistic two-fluid theory.

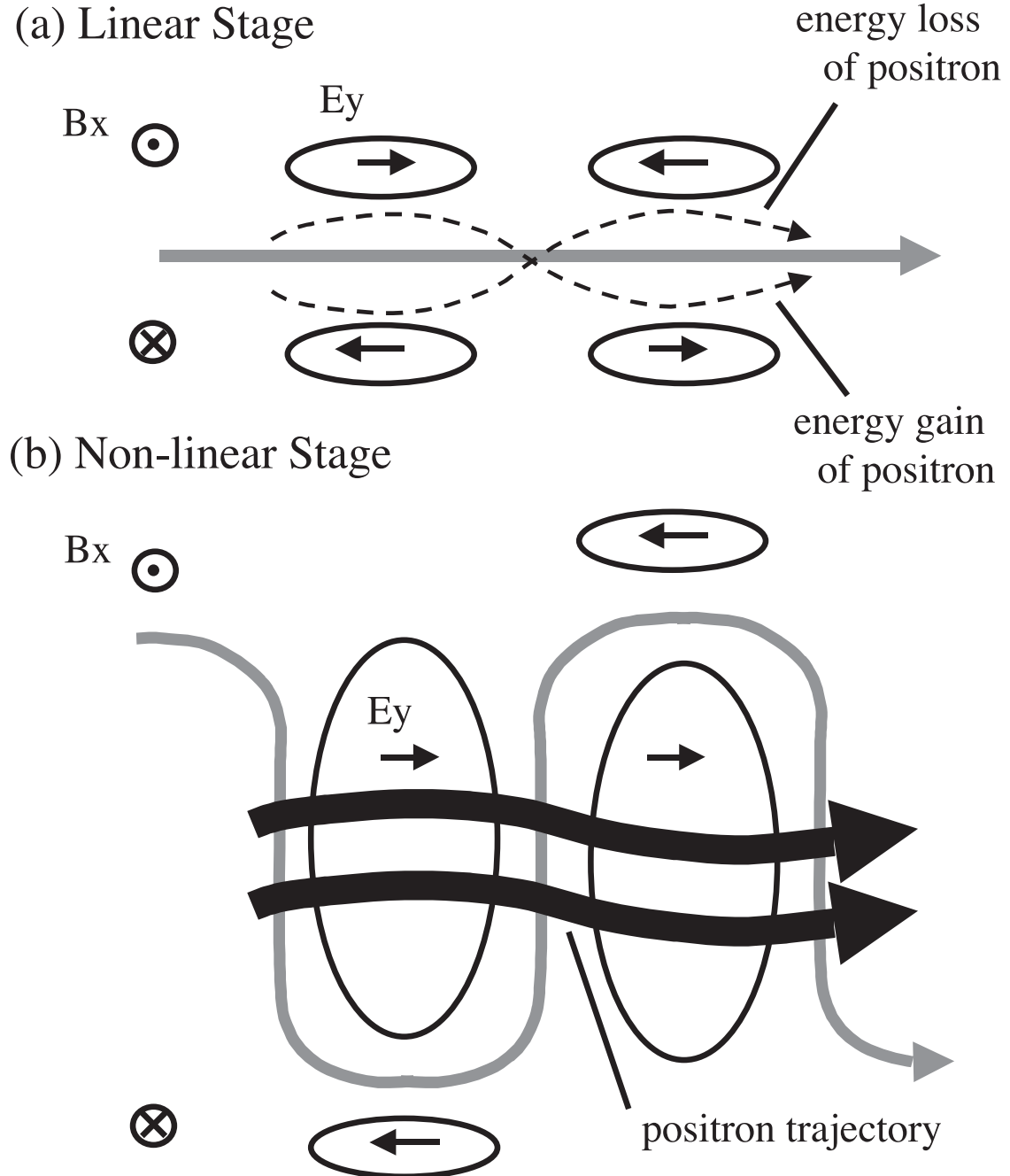


Fig. 3.— Schematic view of the acceleration mechanism. Once the current sheet is folded in the non-linear stage, regions with the positive E_y sign are located in a central acceleration channel.

Run	T	L_x	L_y	L_z	K_{nonth}/K	$\tau_c d \ln(\Delta K)/dt$	ε_{max}	ε_{est}
D1	16	1.0	25.6	51.2	4.7×10^{-2}	2.3×10^{-1}	7.0×10^2	7.1×10^2
D2	1	1.0	25.6	51.2	7.2×10^{-2}	2.3×10^{-1}	4.8×10^1	4.2×10^1
D3	1/16	1.0	25.6	51.2	-	1.9×10^{-2}	4.0	3.0
R1	16	102.4	1.0	51.2	$2.5 \times 10^{-1} <$	6.6×10^{-2}	$3.6 \times 10^3 <$	5.6×10^3
R2	1	102.4	1.0	51.2	$2.6 \times 10^{-1} <$	6.5×10^{-2}	$1.2 \times 10^2 <$	3.5×10^2
R3	1/16	102.4	1.0	51.2	$1.1 \times 10^{-1} <$	7.1×10^{-2}	$5.3 <$	2.2×10^1

Table 1: Three runs for RDKI (D1-3) and relevant runs of relativistic reconnection (R1-3) are presented. The temperature (T/mc^2), the system size (L_x, L_y, L_z in unit of λ), the maximum non-thermal ratio of the kinetic energy (K_{nonth}/K), the energy conversion rate ($\tau_c d \ln(\Delta K)/dt$), the maximum energy (ε_{max}/mc^2) and their estimated values (ε_{est}/mc^2) are presented.